corrosion and materials degradation

MDPI

Supplementary Materials: Indirect Galvanostatic Pulse in Wenner Configuration: Numerical Insights into its Physical Aspect and its Ability to Locate Highly Corroding Areas in Macrocell Corrosion of Steel in Concrete

Romain Rodrigues [1,*], Stéphane Gaboreau [2], Julien Gance [1], Ioannis Ignatiadis [2] and Stéphanie Betelu [2,*]

[1] IRIS Instruments, 1 avenue Buffon, 45100 Orléans, France; j.gance@iris-instruments.com
[2] BRGM, 3 avenue Claude Guillemin, 45060 Orléans Cedex 2, France; s.gaboreau@brgm.fr (S.G.) i.ignatiadis@brgm.fr (I.I.)
* Correspondence: r.rodrigues@iris-instruments.com (R.R.); s.betelu@brgm.fr (S.B.)

Table S1

Table S1. Initial values of the current that polarizes the rebar and the potential difference $V_{P1\text{-}P2}$, corresponding to the ohmic drop, for each input parameters, and the resistivity calculated from $V_{P1\text{-}P2}$ and the total impressed current (I_{C1} = 100 µA) using Equation (6), considering the accurate geometric factor. Similar results were obtained in both active corrosion (i_0 = 0.1 A m^{-2}) and passive corrosion (i_0 = 10^{-5} A m^{-2}), which indicates that the instantaneous ohmic drop is independent on the electrochemical state of the rebar. However, a small difference between the two electrochemical states (3.3%) was observed for a = 2.5 cm.

a (cm)	e (mm)	Φ (mm)	ρ (Ω m)	I_{rebar} (µA)	$V_{P1\text{-}P2}$ (mV)	ρ_{calc} (Ω m)	% of underestimation
2.5	40	12	100	43.87	60.18	89.71	10.29
			200	43.87	120.4	179.4	
			500	43.87	300.9	448.5	
			1000	43.88	601.8	897.1	
5	**40**	**12**	100	64.32	22.56	68.50	31.50
			200	64.32	45.11	137.0	
			500	64.32	112.8	342.5	
			1000	64.32	225.5	685.0	
7.5	40	12	100	74.39	10.35	40.04	59.96
			200	74.39	20.70	80.08	
			500	74.39	51.75	200.2	
			1000	74.39	103.5	400.4	
10	40	12	100	80.17	5.520	23.43	76.57
			200	80.18	11.04	46.85	
			500	80.18	27.60	117.1	
			1000	80.18	55.19	234.2	
15	40	12	100	87.15	2.288	9.267	90.73
			200	87.15	4.575	18.53	
			500	87.15	11.44	46.32	
			1000	87.15	22.87	92.63	
5	**20**	12	100	82.03	8.511	25.85	74.15
			200	82.03	17.02	51.68	
			500	82.04	42.54	129.2	
			1000	82.04	85.07	258.4	
5	**60**	12	100	52.09	29.08	88.32	11.68
			200	52.09	58.16	176.6	
			500	52.09	145.4	441.6	
			1000	52.09	290.8	883.2	
5	40	**6**	100	58.09	23.55	71.52	28.48
			200	58.10	47.10	143.0	
			500	58.10	117.8	357.6	
			1000	58.10	235.5	715.1	
5	40	**25**	100	71.80	21.74	66.03	33.97
			200	71.81	43.49	132.1	
			500	71.81	108.7	330.2	
			1000	71.81	217.4	660.3	

Table S1bis. Effect of the impressed current on the ohmic drop and the calculated concrete resistivity. Initial values of the current that polarizes the rebar and the potential difference $V_{P1\text{-}P2}$, corresponding to the ohmic drop, for each input parameters, and the resistivity calculated from $V_{P1\text{-}P2}$ and the total impressed current using Equation (6), considering the accurate geometric factor. In agreement with Ohm's law, there is no effect of the value of the impressed current on concrete resistance, and thus on concrete resistivity.

a (cm)	e (mm)	Φ (mm)	I_{C1} (µA)	ρ (Ω m)	I_{rebar} (µA)	$V_{P1\text{-}P2}$ (mV)	ρ_{calc} (Ω m)
5	40	12	100	100	64.32	22.56	68.50
				200	64.32	45.11	137.0
				500	64.32	112.8	342.5
				1000	64.32	225.5	685.0
			300	100	193.0	67.67	68.50
				200	193.0	135.3	137.0
				500	193.0	338.3	324.5
				1000	193.0	676.6	685.0
			500	100	321.6	112.8	68.50
				200	321.6	225.6	137.0
				500	321.6	563.9	342.5
				1000	321.6	1128	685.0

Figure S1

Figure S1 presents further experimental results obtained on unreinforced mortar samples in four-electrode configuration using the indirect GP technique (Fig. S1A), the conventional three-electrode configuration GP technique (Fig. S1B), and the indirect EIS technique (Figs. S1C and S1D).

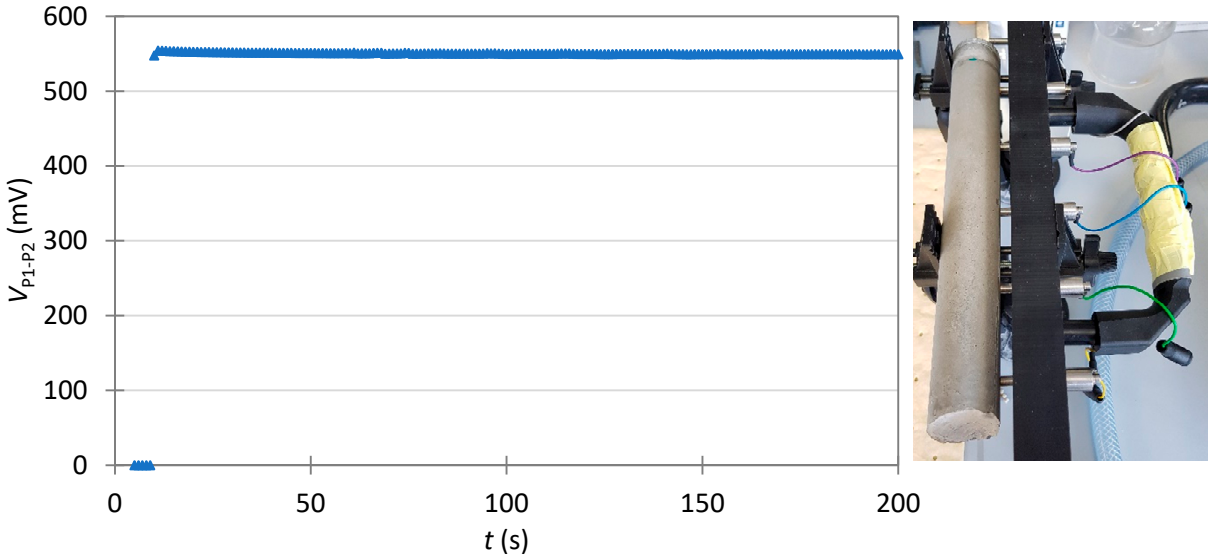

Figure S1A. Evolution of V_{P1-P2} with time in the case of a small unreinforced specimen showing only an ohmic drop, indicating that the polarization observed on reinforced specimen is related to the rebar.

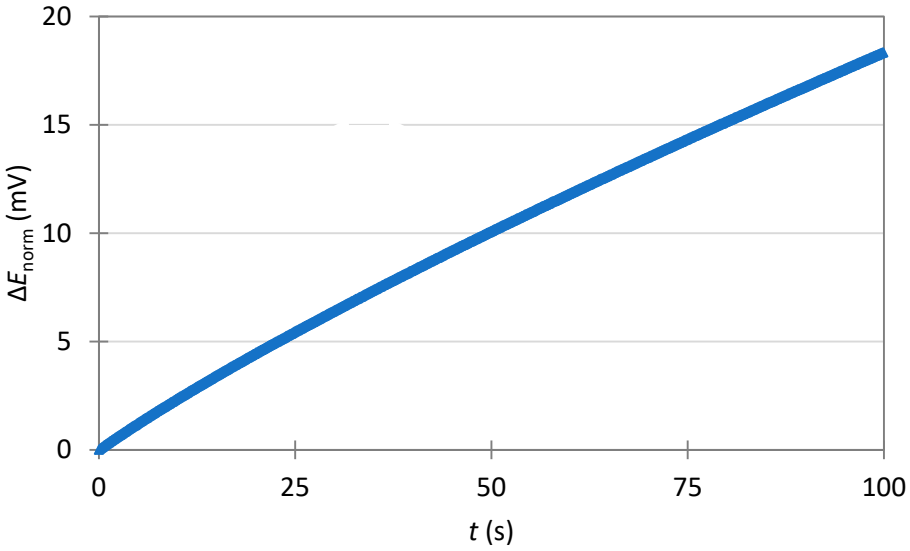

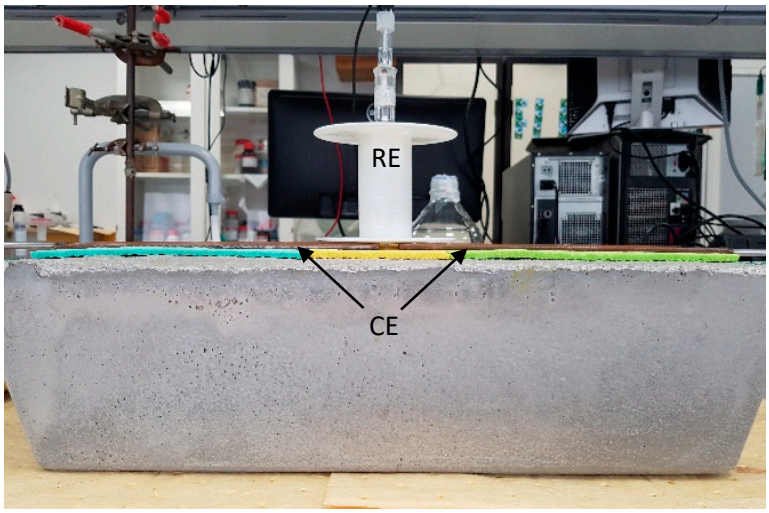

Figure S1B. Evolution of *V* with time obtained in the three-electrode configuration using the GP technique for the passive rebar with *I* = 5 μA. The results indicate that the quasi-steady-state is far from being reached after 100 s in this configuration.

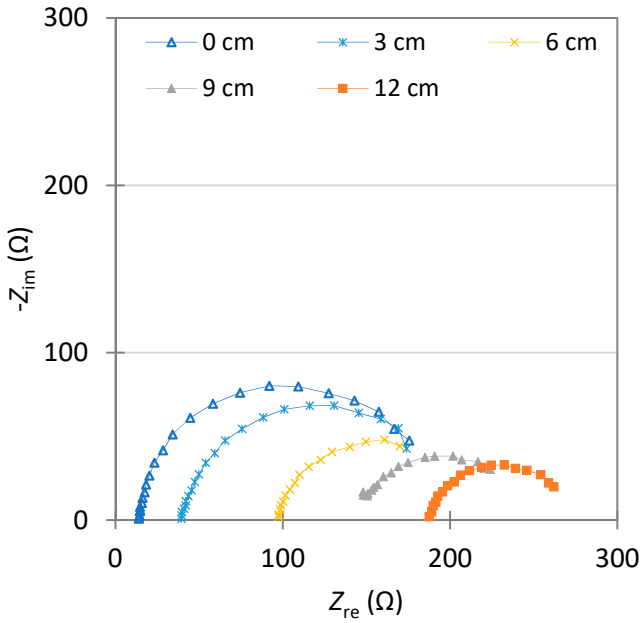

Figure S1C. Influence of the distance of the monitoring device from the rebar with a = 15 cm using indirect EIS technique for the passive rebar. 0 cm = measurements above and parallel to the rebar. The further the monitoring device is from the rebar, the higher the measured apparent concrete resistivity and the lower the measured apparent polarization resistance.

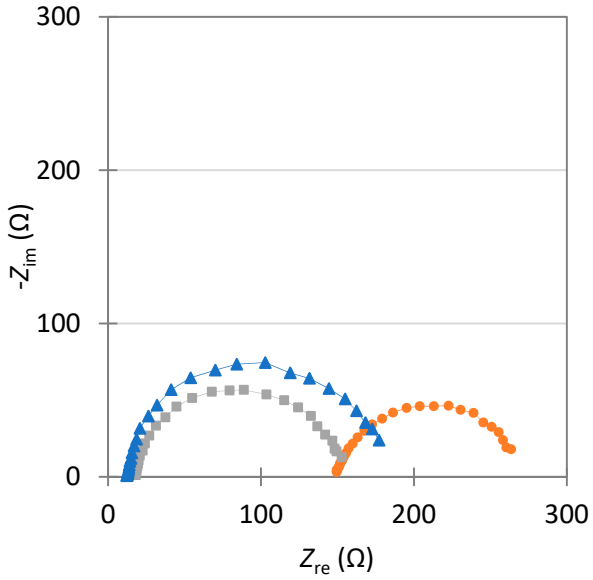

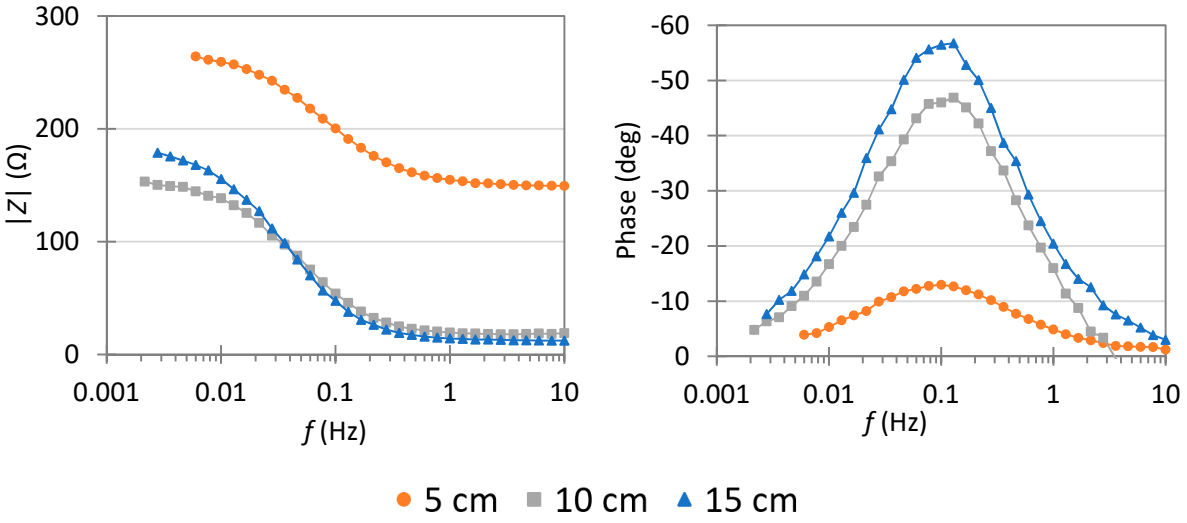

Figure S1D. Influence of the probe spacing on the potential response using the indirect EIS technique for the passive rebar. The increase in the probe spacing decreases the measured apparent resistivity (at high frequency) and increases the measured polarization resistance (at low frequency). Only a small difference is observed between 10 cm and 15 cm for the apparent resistivity due to the small size of the element, which affects the distribution of the current in the material (border effects).

Figure S2

A - Effect of the probe spacing *a*:

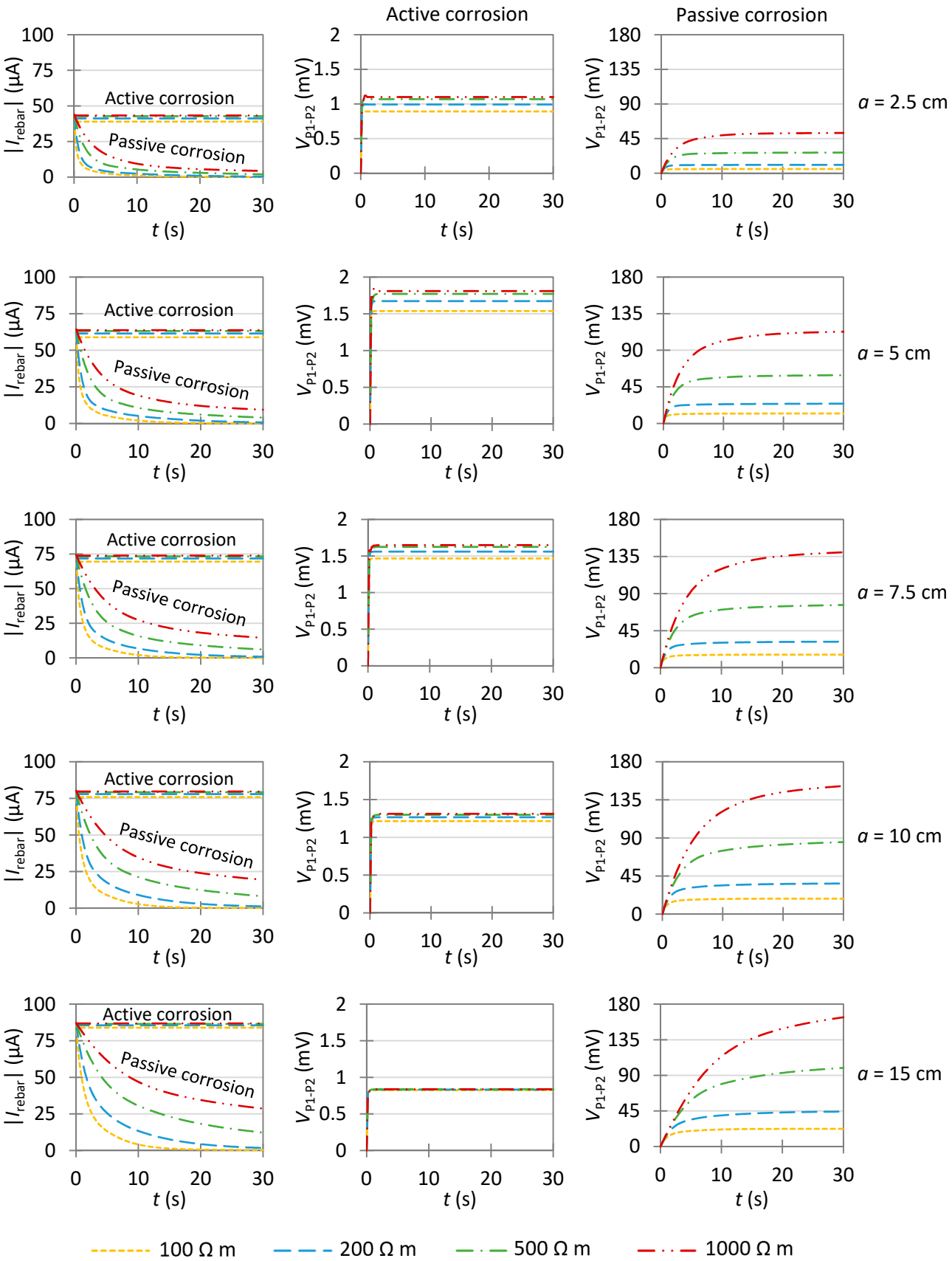

B - Effect of the cover depth *e*:

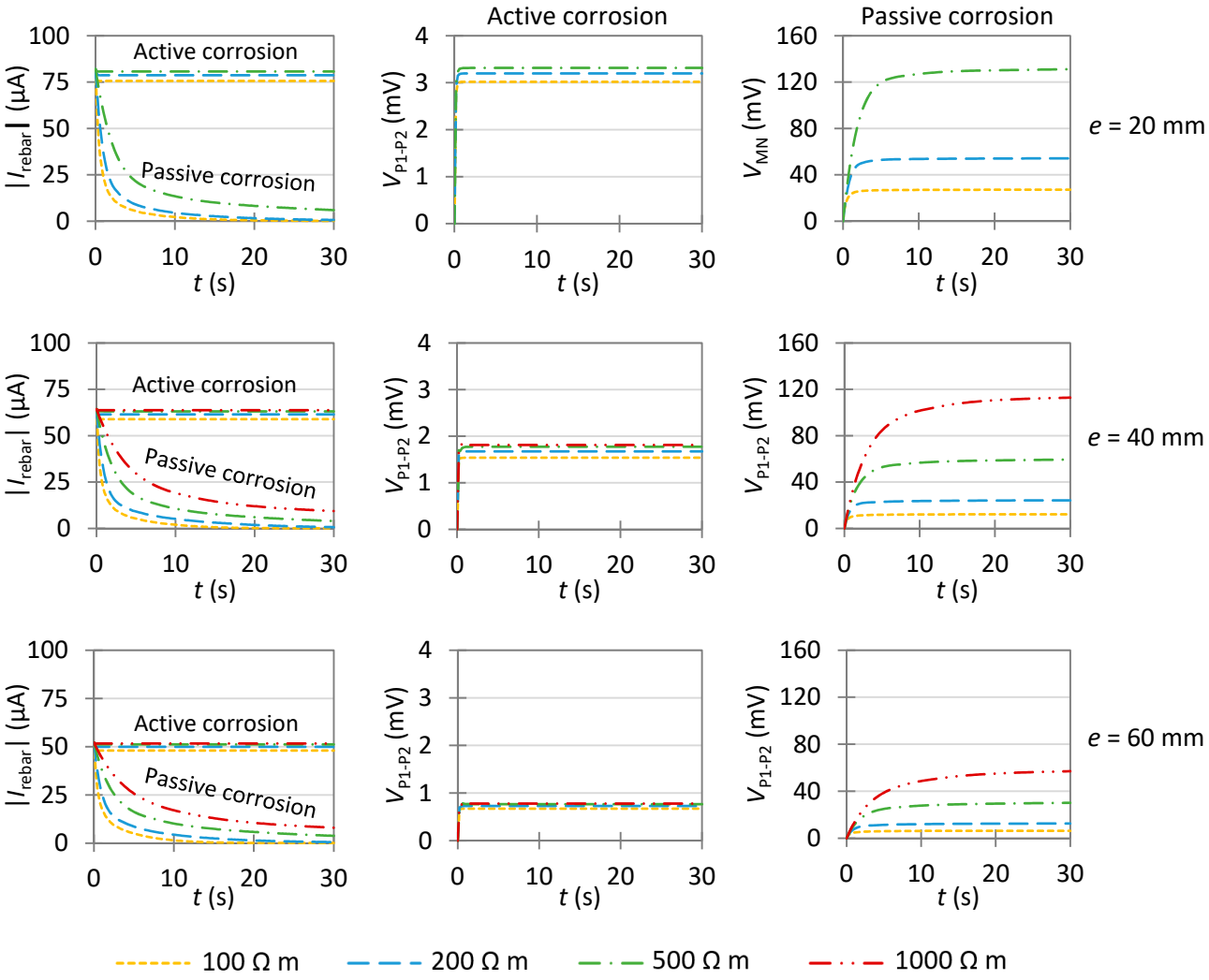

C – Effect of the rebar diameter Φ:

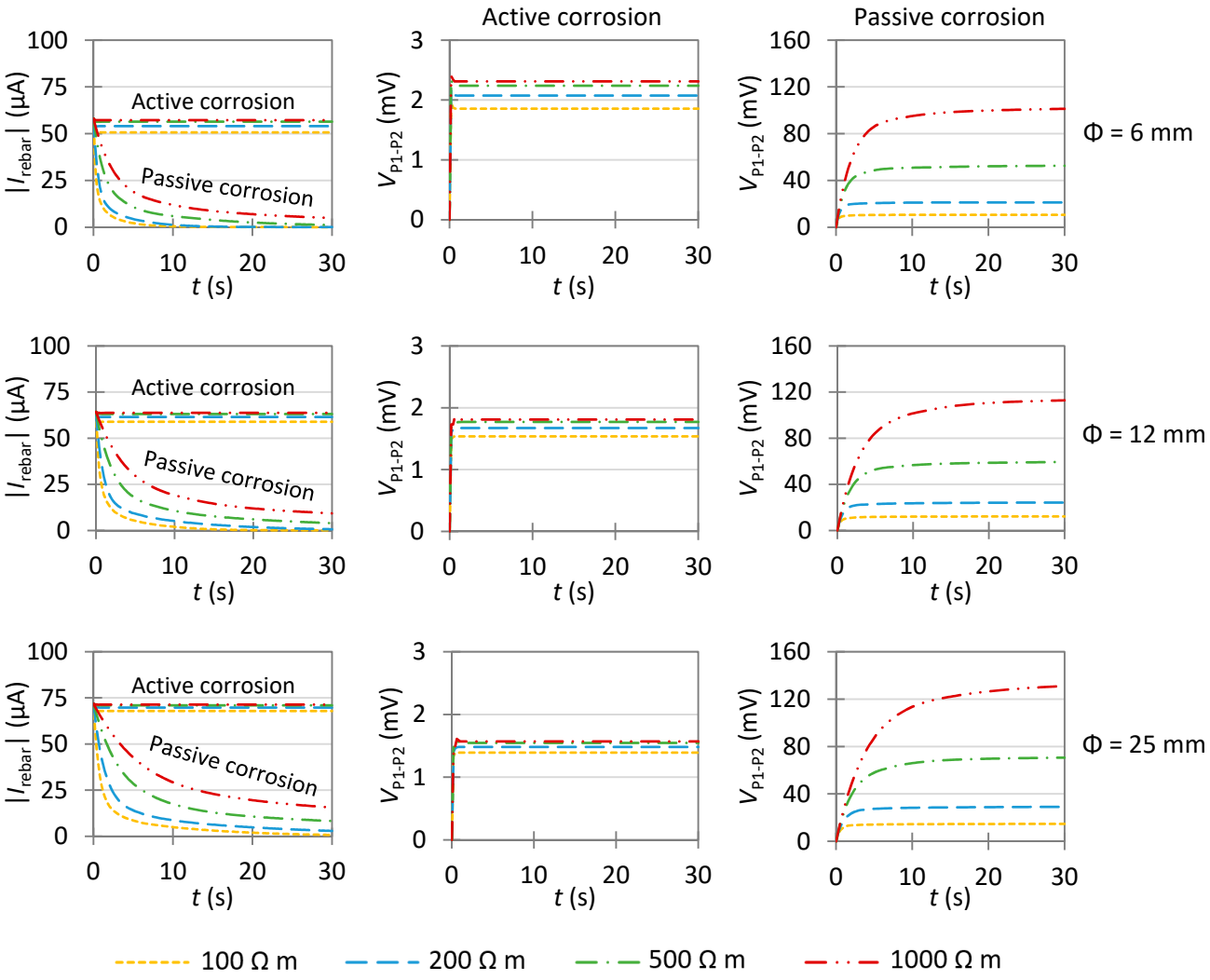

D – Effect of the impressed current I_{C1}:

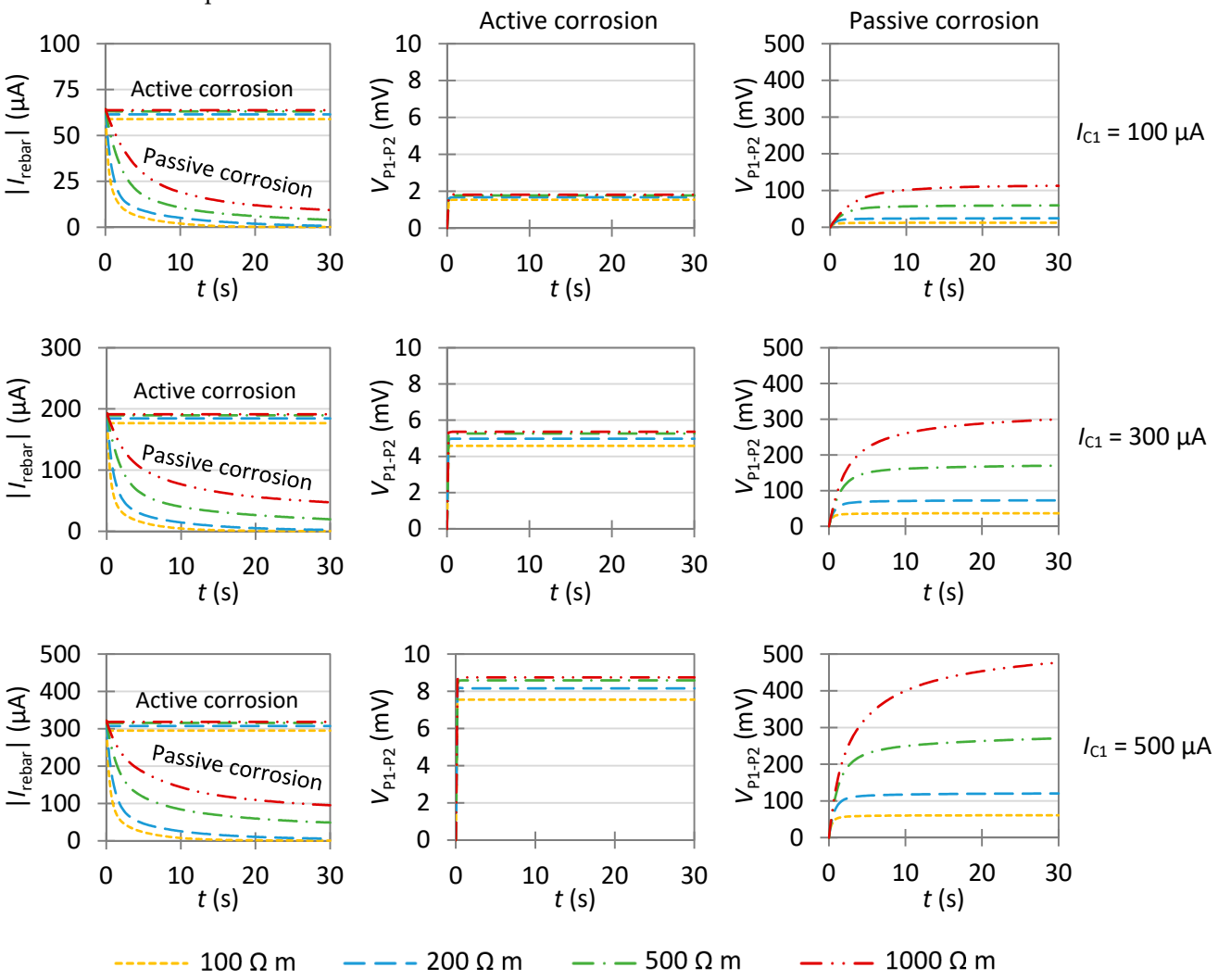

Figure S2. Evolution of I_{rebar} and $V_{P1\text{-}P2}$ when considering uniform corrosion, in active ($i_{0,a}$ = 0.1 A m^{-2}) or passive states ($i_{0,c}$ = 10^{-5} A m^{-2}) with C_{dl} = 0.2 F m^{-2}. Input parameters:

- A: e = 40 mm, Φ = 12 mm, I_{C1} = 100 μA, while a = 2.5, 5, 7.5, 10 or 15 cm;
- B: a = 5 cm, Φ = 12 mm, I_{C1} = 100 μA, while e = 20, 40 or 60 mm;
- C: a = 5 cm, e = 40 mm, I_{C1} = 100 μA, while Φ = 6, 12 or 25 mm;
- D: a = 5 cm, e = 40 mm, Φ = 12 mm, while I_{C1} = 100, 300 or 500 μA.

Figure S3

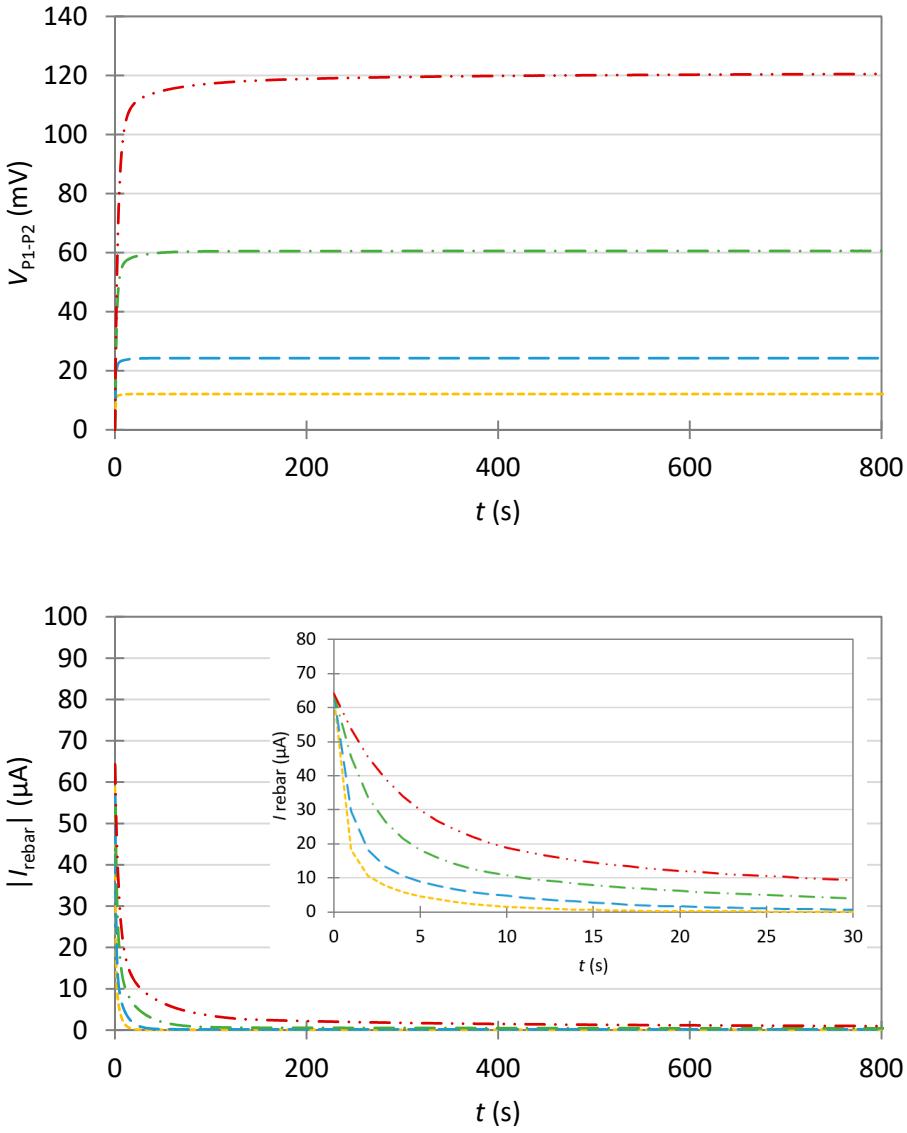

Figure S3. Evolution of V_{P1-P2} and I_{rebar} during 800 s for a passive rebar. Input parameters: $i_0 = 10^{-5}$ A m^{-2}, a = 5 cm, e = 40 mm, Φ = 12 mm, C_{dl} = 0.2 F m^{-2}, I_{C1} = 100 μA. The time required to reach the steady state increases when increasing concrete resistivity.

Figure S4

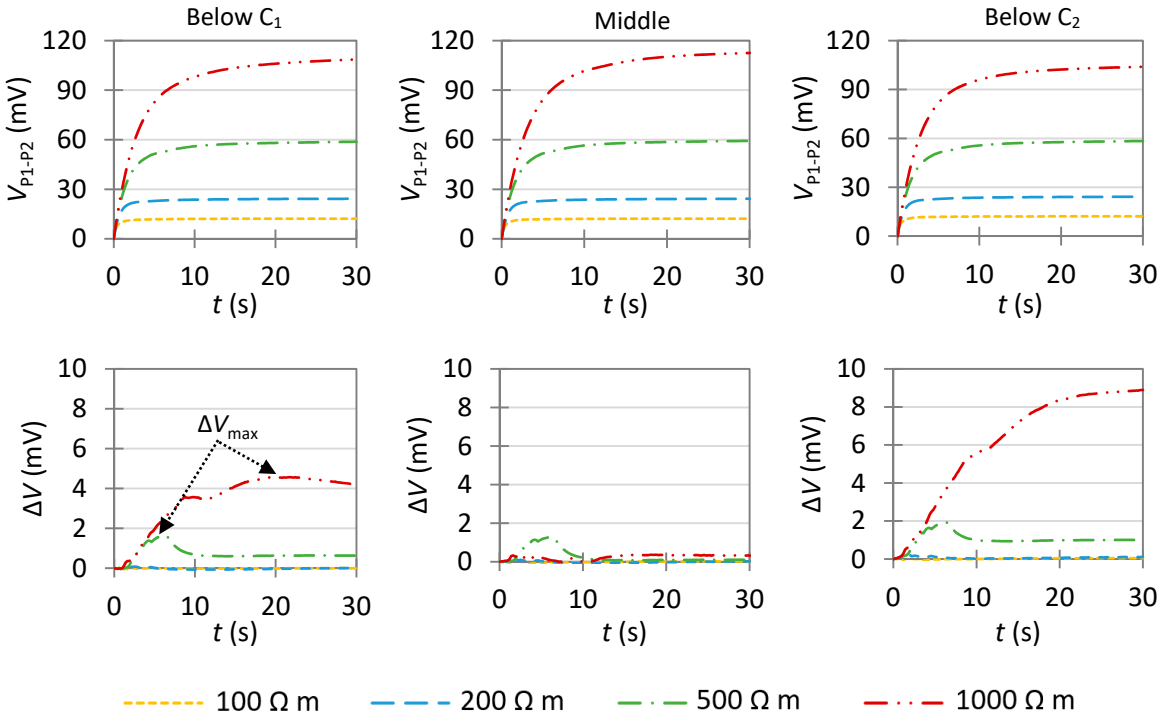

Figure S4. Evolution of $V_{P1\text{-}P2}$ and ΔV over time in the presence of a slightly corroding area at different positions relative to the monitoring device. Input parameters: $i_{0,a} = 10^{-4}$ A m^{-2}, $i_{0,c} = 10^{-5}$ A m^{-2}, $L_a = 3$ cm, $a = 5$ cm, $e = 40$ mm, $C_{dl} = 0.2$ F m^{-2}, $I_{C1} = 100$ μA.

Figure S5

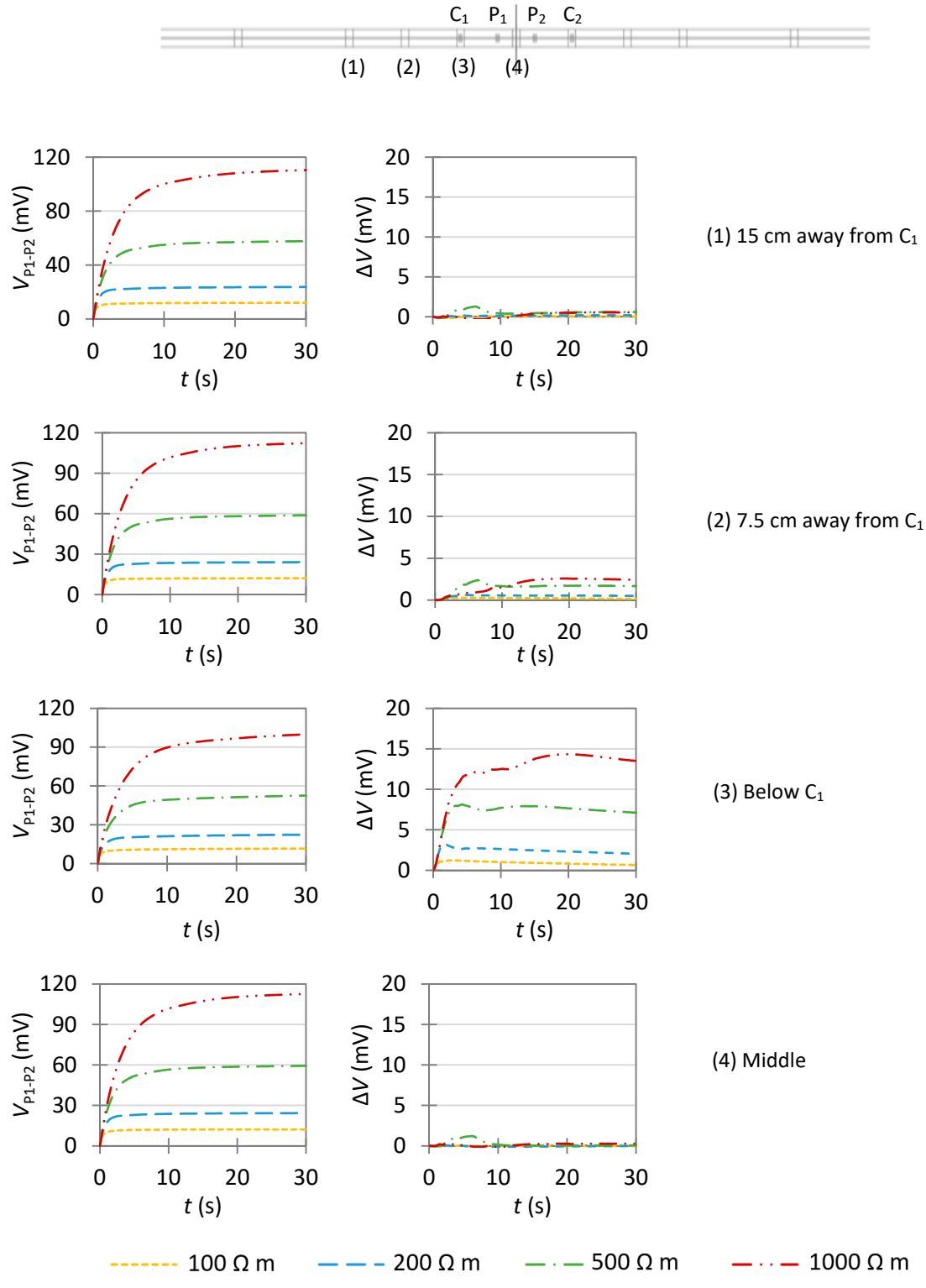

Figure S5A. Evolution of $V_{P1\text{-}P2}$ and ΔV over time in the presence of a highly corroding area at different positions relative to the monitoring device. Input parameters: $i_{0,a} = 0.1$ A m^{-2}, $i_{0,c} = 10^{-5}$ A m^{-2}, $L_a = 1$ cm, $a = 5$ cm, $e = 40$ mm, $C_{dl,a} = C_{dl,c} = 0.2$ F m^{-2}, $I_{C1} = 100$ µA.

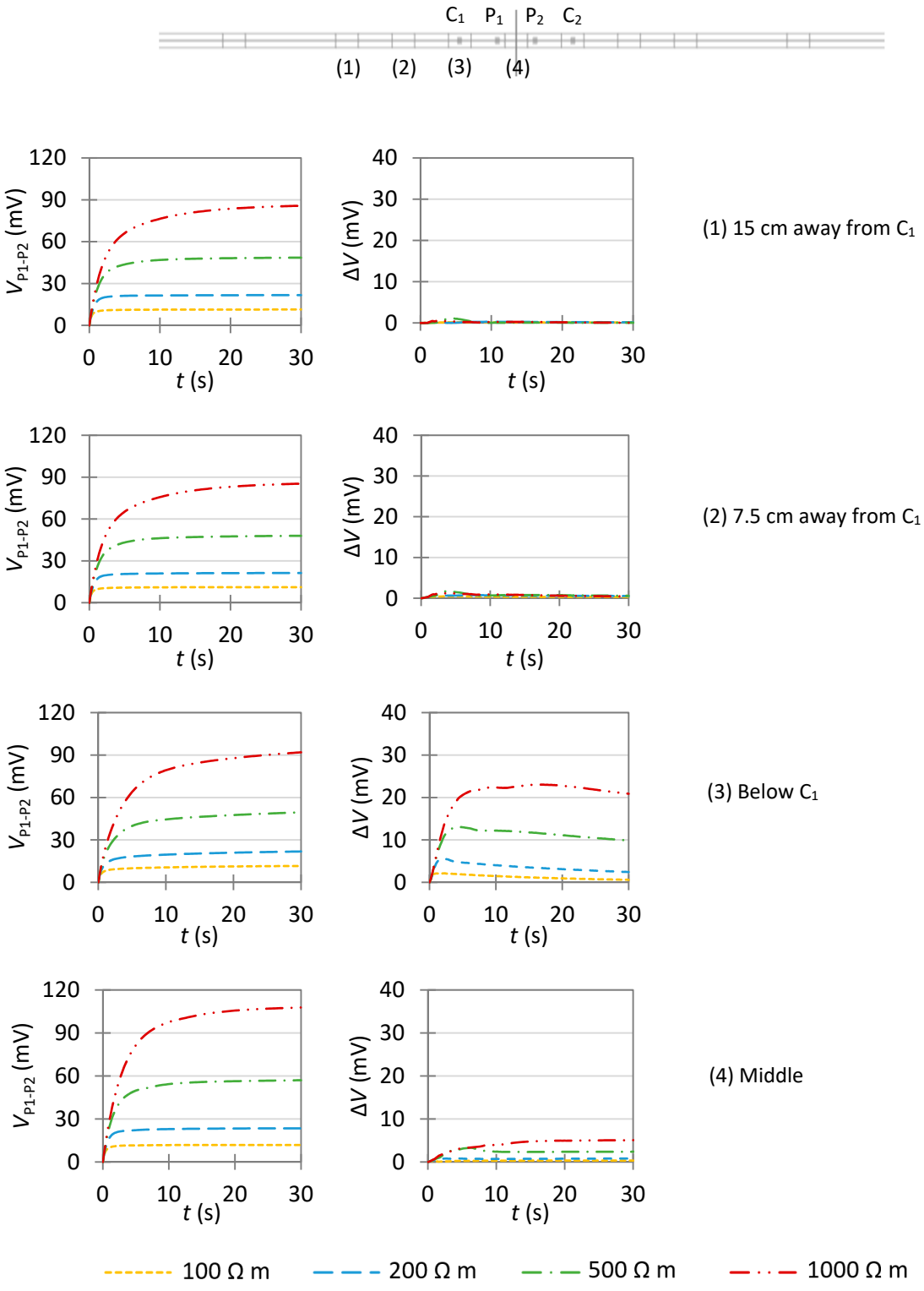

Figure S5B. Evolution of V_{P1-P2} and ΔV over time in the presence of a highly corroding area at different positions relative to the monitoring device. Input parameters: $i_{0,a}$ = 0.1 A m^{-2}, $i_{0,c}$ = 10^{-5} A m^{-2}, L_a = 3 cm, a = 5 cm, e = 40 mm, $C_{dl,a}$ = $C_{dl,c}$ = 0.2 F m^{-2}, I_{C1} = 100 μA.

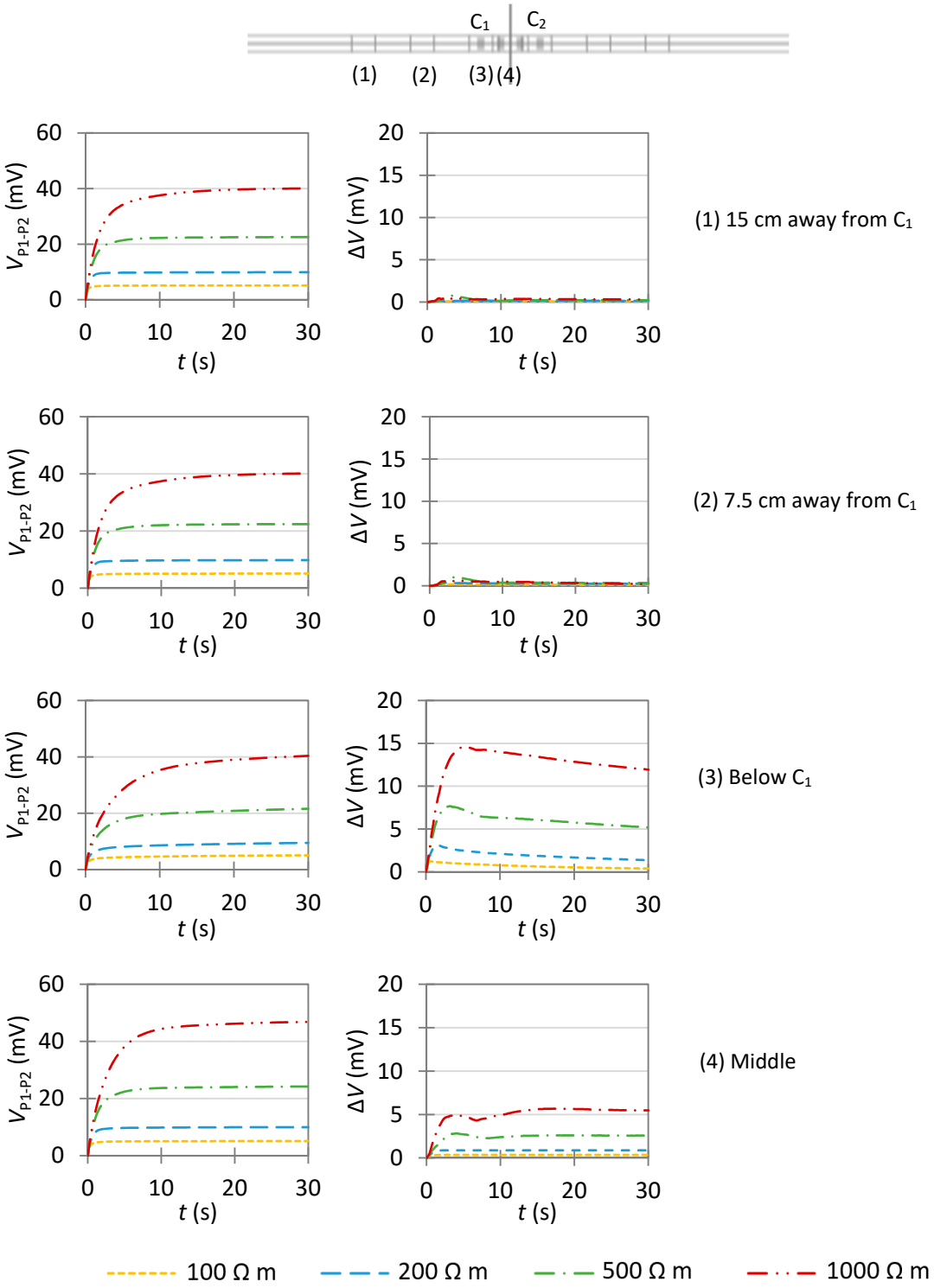

Figure S5C. Evolution of $V_{P1\text{-}P2}$ and ΔV over time in the presence of a highly corroding area at different positions relative to the monitoring device. Input parameters: $i_{0,a} = 0.1$ A m^{-2}, $i_{0,c} = 10^{-5}$ A m^{-2}, $L_a = 3$ cm, $a = 2.5$ cm, $e = 40$ mm, $C_{dl,a} = C_{dl,c} = 0.2$ F m^{-2}, $I_{C1} = 100$ µA.

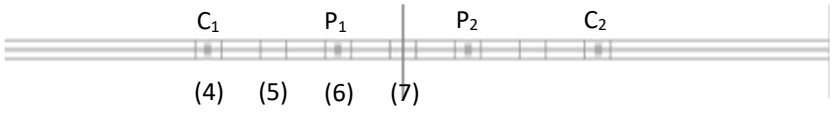

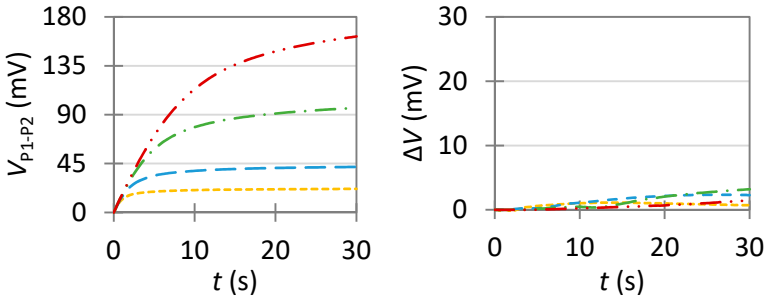

(1) 30 cm away from C_1

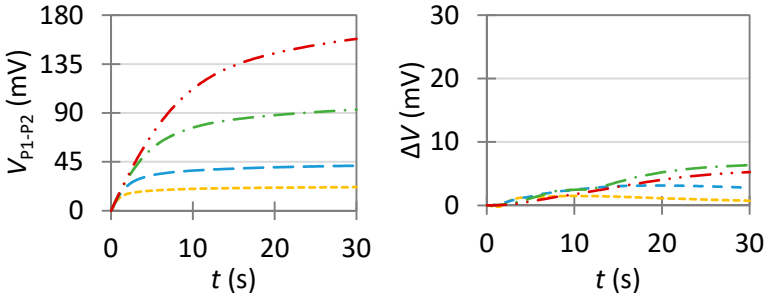

(2) 15 cm away from C_1

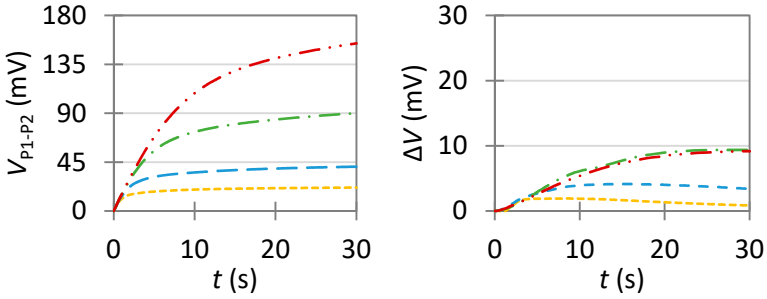

(3) 7.5 cm away from C_1

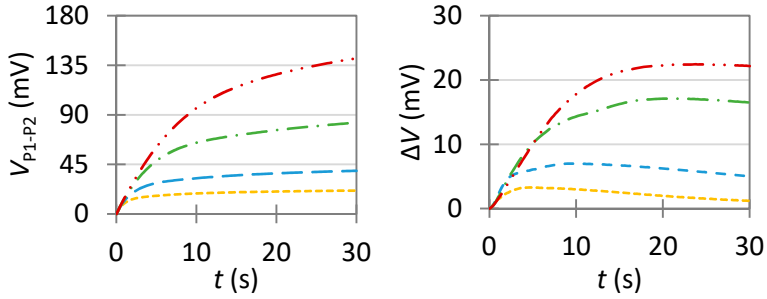

(4) Below C_1

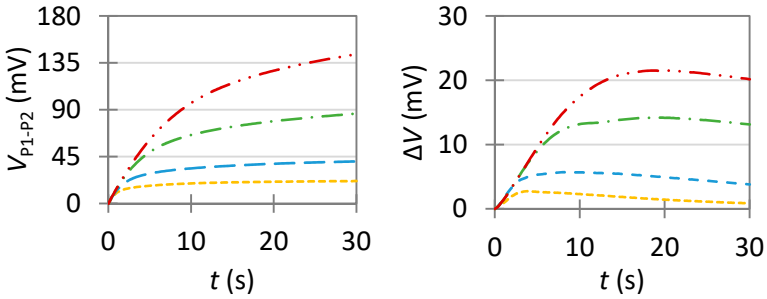

(5) 7.5 cm away from P_1

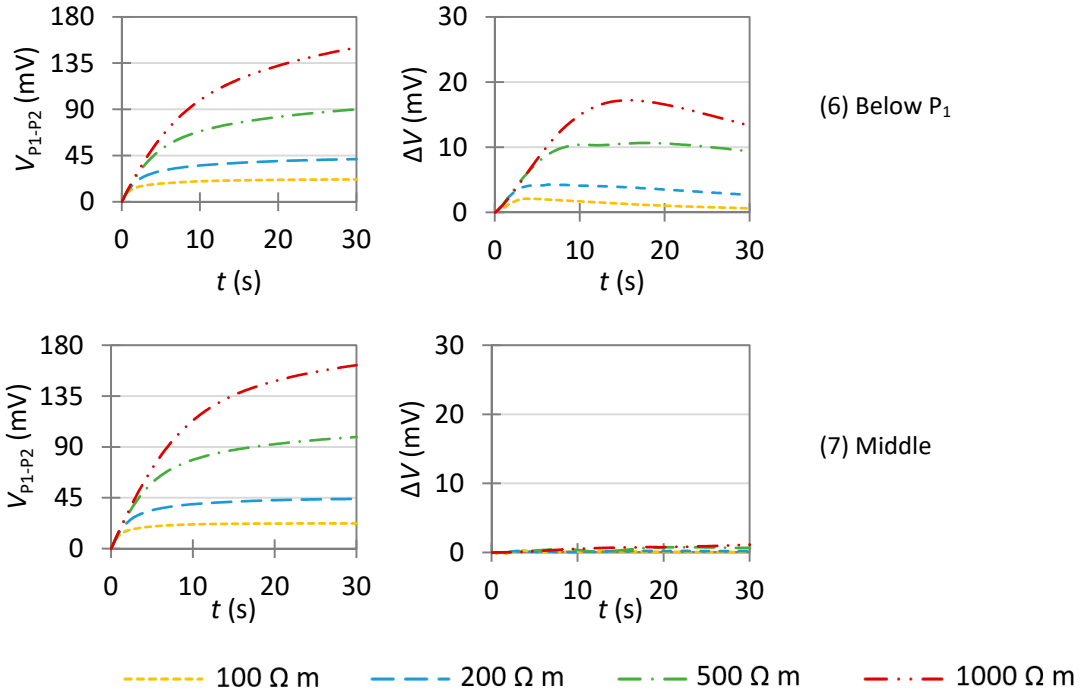

Figure S5D. Evolution of V_{P1-P2} and ΔV over time in the presence of a highly corroding area at different positions relative to the monitoring device. Input parameters: $i_{0,a} = 0.1$ A m^{-2}, $i_{0,c} = 10^{-5}$ A m^{-2}, $L_a = 3$ cm, $a = 15$ cm, $e = 40$ mm, $C_{dl,a} = C_{dl,c} = 0.2$ F m^{-2}, $I_{C1} = 100$ µA.

Figure S6

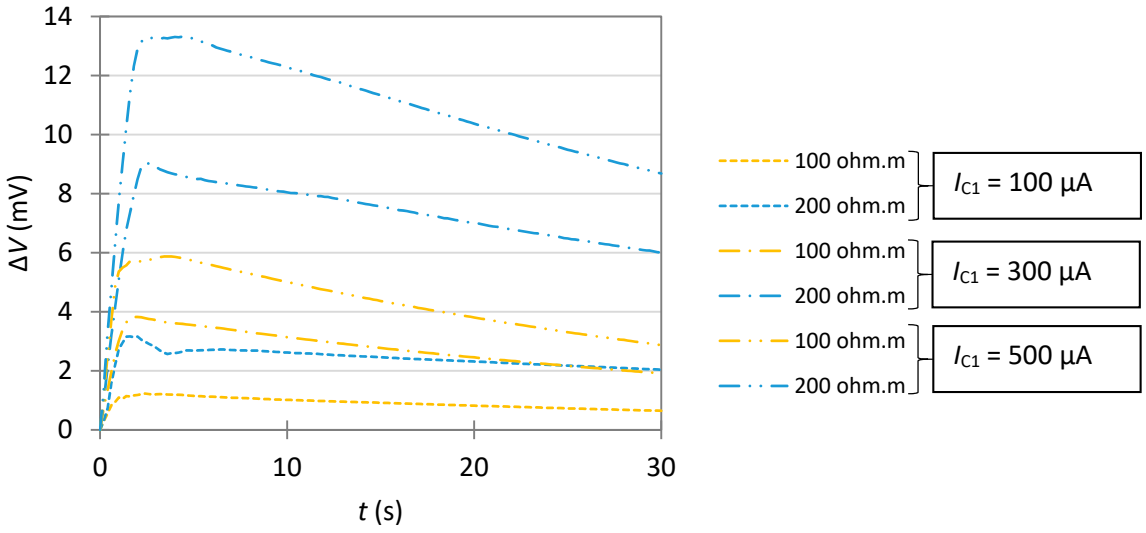

Figure S6. Influence of the impressed current I_{C1} on ΔV when the anode is below C_1 for ρ = 100 or 200 Ω m. ΔV_{max} increases when increasing I_{C1}, which allows a better detection of the highly corroding area.

Figure S7

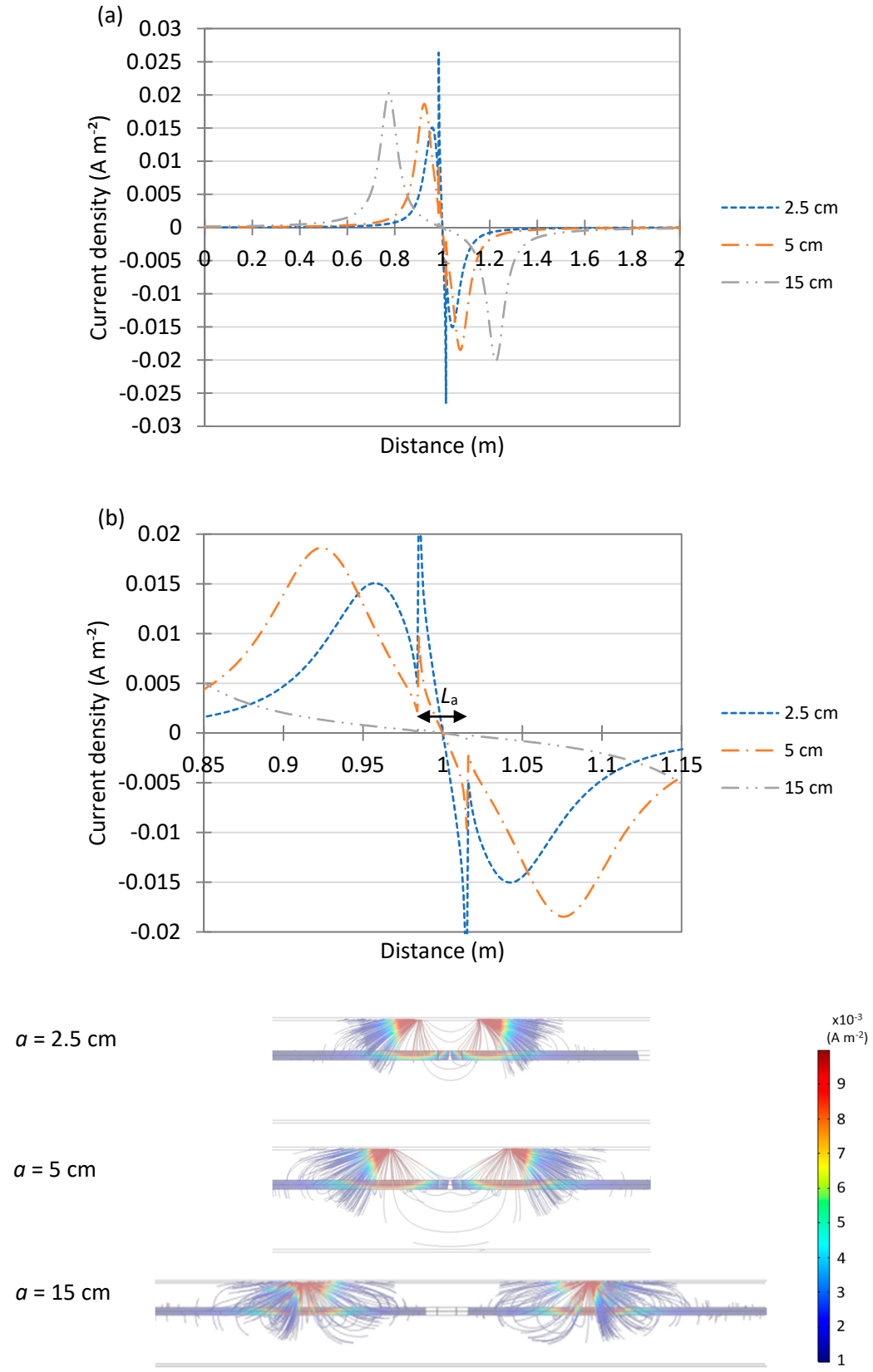

Figure S7. Effect of the probe spacing on the distribution of the normal current density, evaluated here at 0.2 s, along the upper ridge of the rebar (the most polarized ridge). Input parameters: $i_{0,a}$ = 0.1 A m^{-2}, $i_{0,c}$ = 10^{-5} A m^{-2}, ρ = 200 Ω m, L_a = 3 cm, e = 40 mm, $C_{dl,a}$ = $C_{dl,c}$ = 0.2 F m^{-2}, I_{C1} = 100 μA. The figure (b) is a zoom on the central part of the rebar, where the length L_a and position of the anode are indicated.

Figure S8

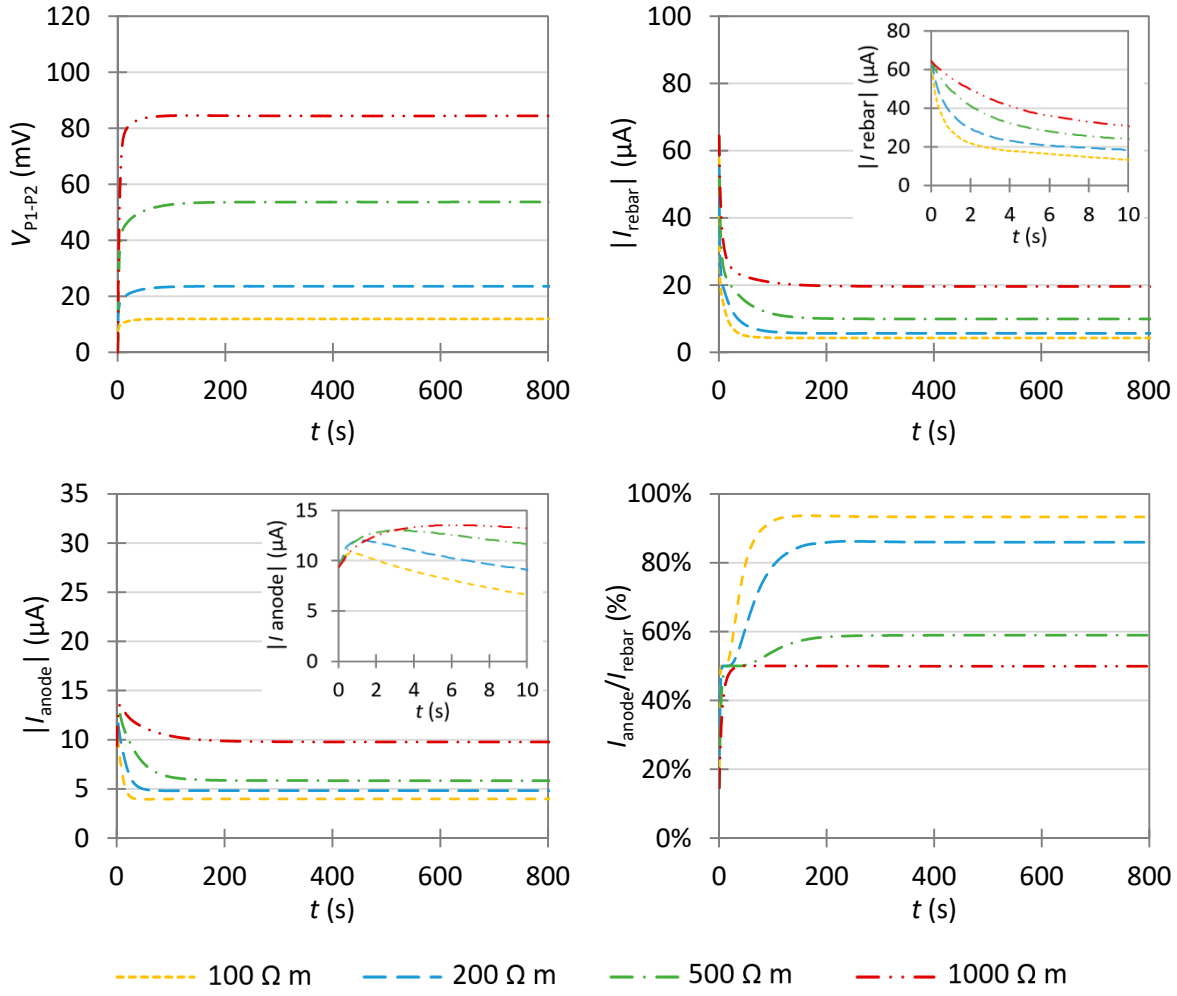

Figure S8A. Evolution of V_{P1-P2}, I_{rebar}, I_{anode}, and I_{anode}/I_{rebar} over time when the anode is below C_2. Input parameters: $i_{0,a} = 0.1$ A m^{-2}, $i_{0,c} = 10^{-5}$ A m^{-2}, $L_a = 3$ cm, $a = 5$ cm, $e = 40$ mm, $C_{dl,a} = C_{dl,c} = 0.2$ F m^{-2}, $I_{C1} = 100$ μA.

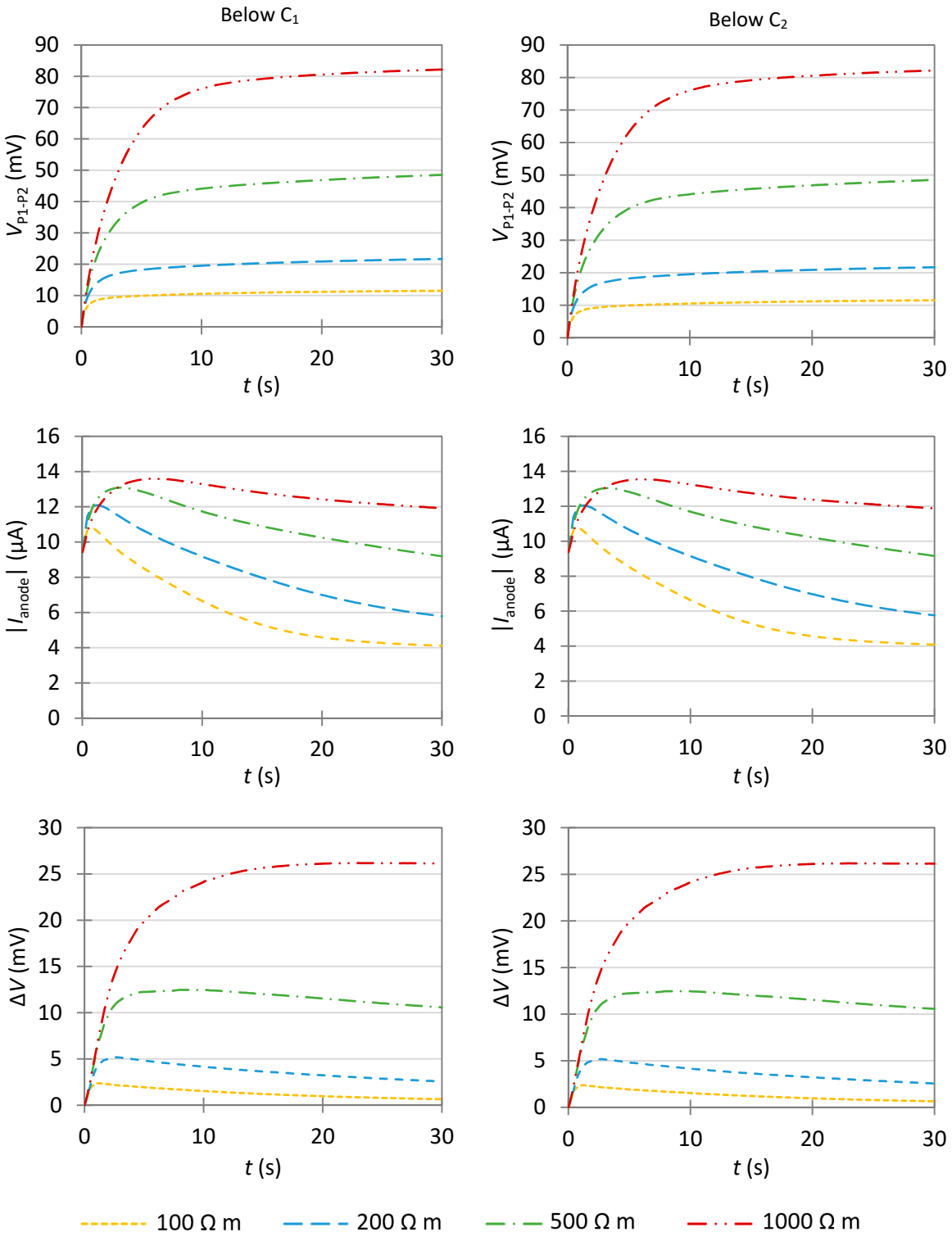

Figure S8B. Evolution of $V_{P1\text{-}P2}$, I_{anode} and ΔV over time when the anode is below C_1 or below C_2, considering the same anodic charge transfer coefficient for anodic and cathodic areas ($\alpha_a = 0.012$). Input parameters: $i_{0,a} = 0.1$ A m^{-2}, $L_a = 3$ cm, $a = 5$ cm, $e = 40$ mm, $C_{dl} = 0.2$ F m^{-2}, $I_{C1} = 100$ µA.

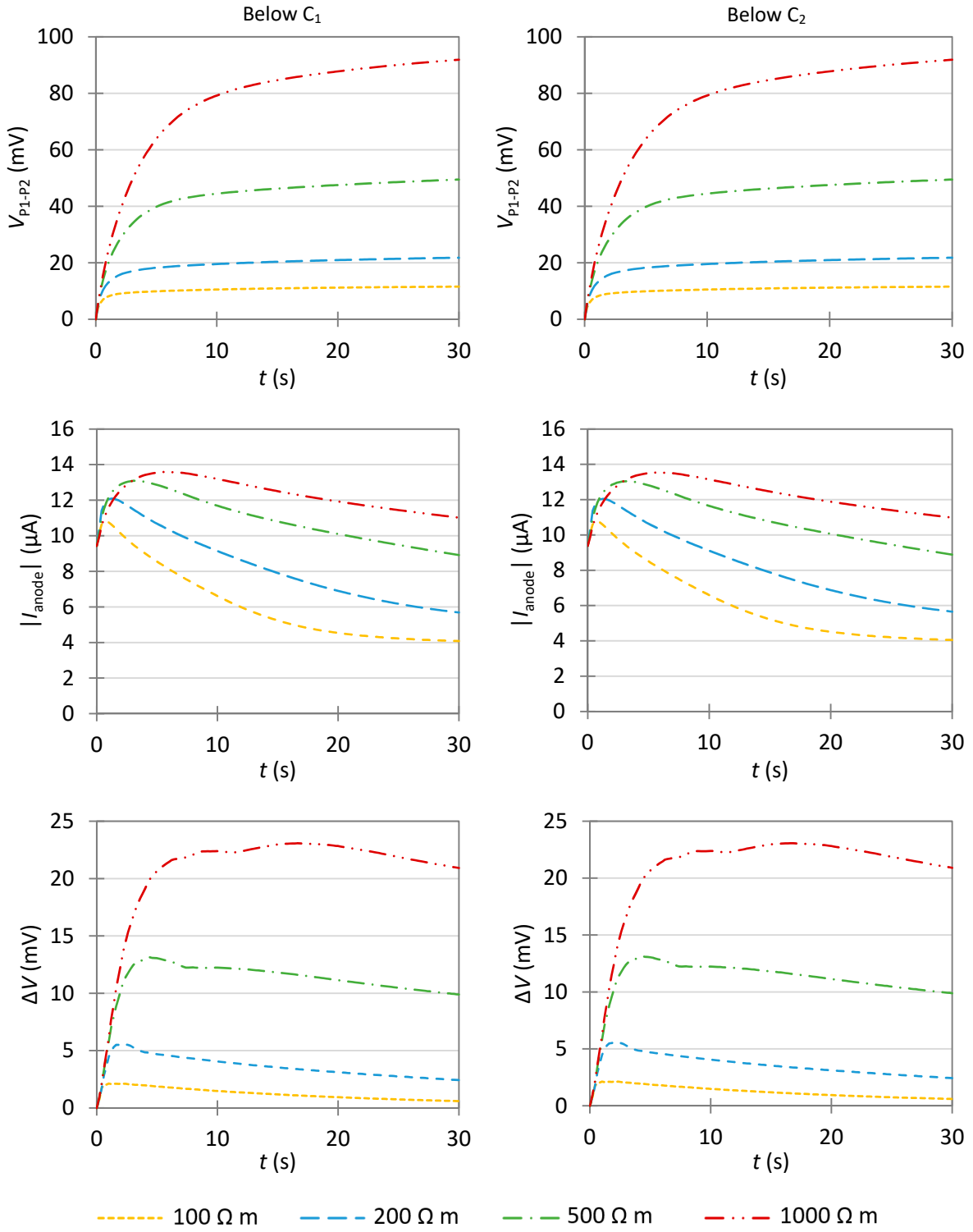

Figure S8C. Evolution of $V_{P1\text{-}P2}$, I_{anode} and ΔV over time when the anode is below C_1 or C_2, considering the same anodic charge transfer coefficient for anodic and cathodic areas (α_a = 0.5). Input parameters: $i_{0,a}$ = 0.1 A m^{-2}, L_a = 3 cm, a = 5 cm, e = 40 mm, C_{dl} = 0.2 F m^{-2}, I_{C1} = 100 µA.

Figure S9

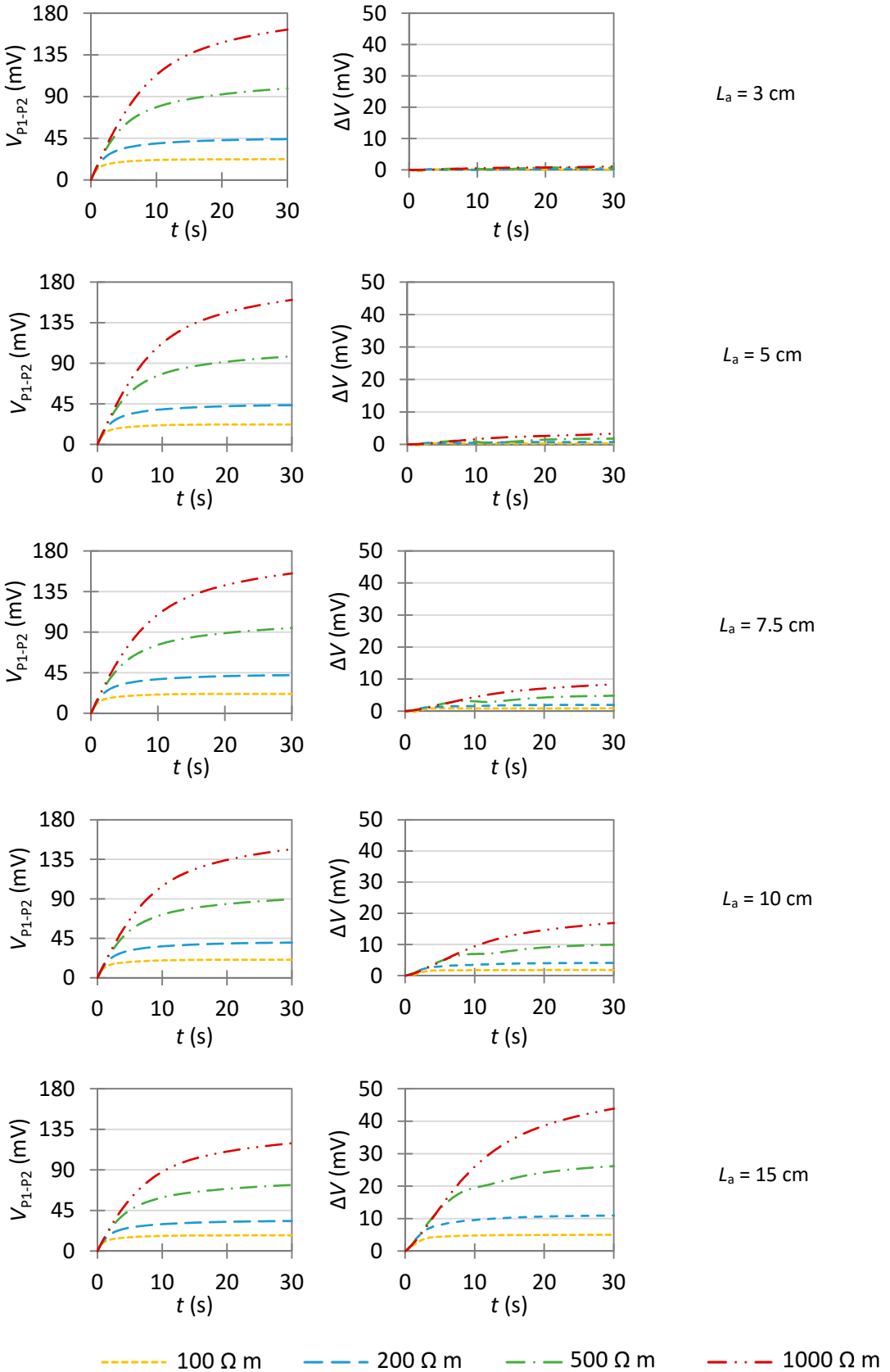

Figure S9. Evolution of V_{P1-P2} and ΔV over time in the presence of a highly corroding area centred between P_1 and P_2, for several length L_a. Input parameters: $i_{0,a} = 0.1$ A m^{-2}, $i_{0,c} = 10^{-5}$ A m^{-2}, $a = 15$ cm, $e = 40$ mm, $C_{dl,a} = C_{dl,c} = 0.2$ F m^{-2}, $I_{C1} = 100$ µA.

Figure S10

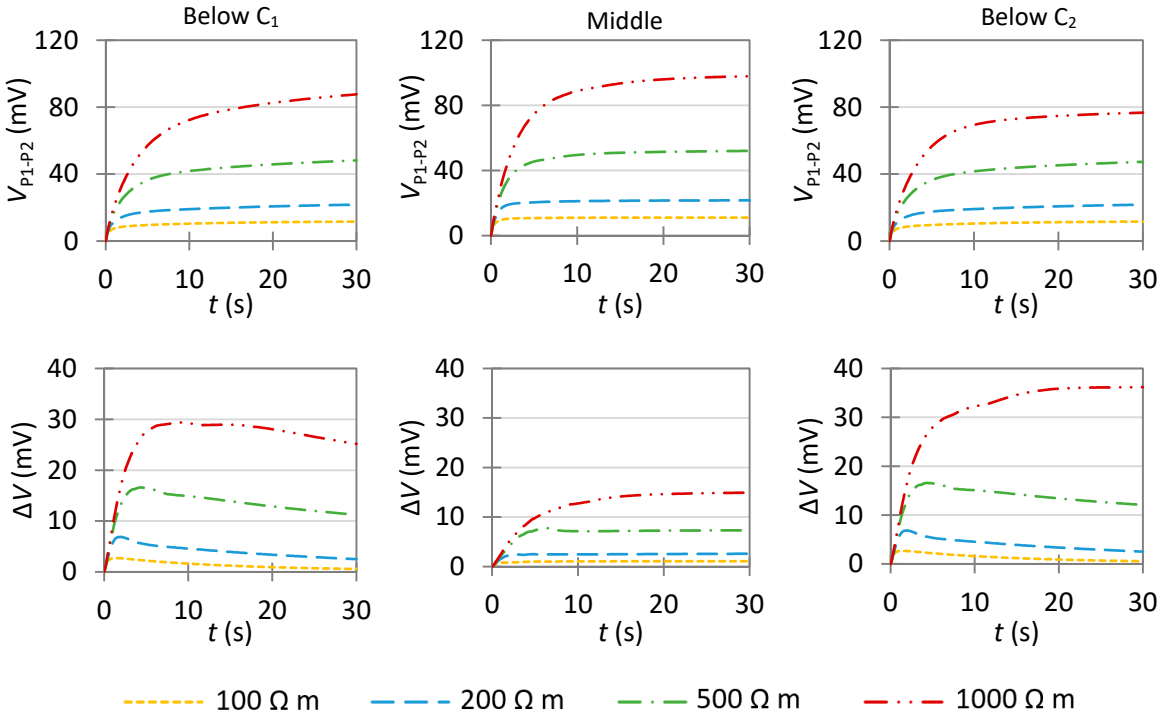

Figure S10A. Evolution of $V_{P1\text{-}P2}$ and ΔV over time in the presence of a highly corroding area at different positions relative to the monitoring device. Input parameters: $i_{0,a}$ = 0.1 A m^{-2}, $i_{0,c}$ = 10^{-5} A m^{-2}, L_a = 5 cm, a = 5 cm, e = 40 mm, C_{dl} = 0.2 F m^{-2}, I_{C1} = 100 µA.

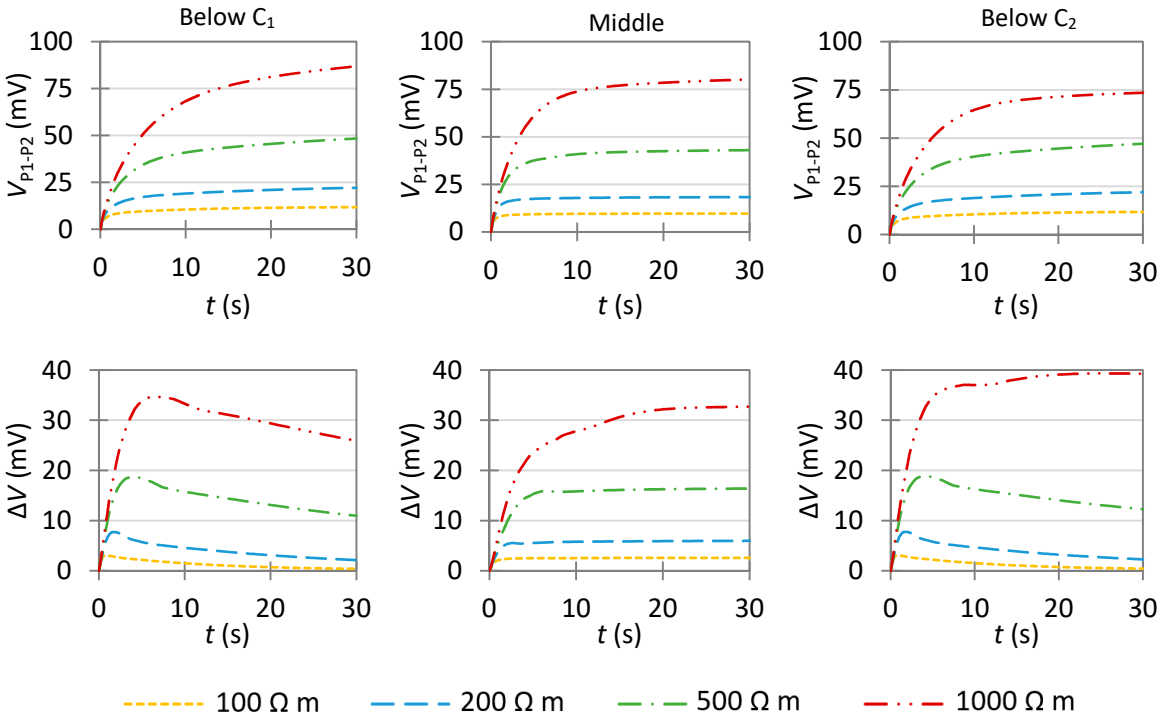

Figure S10B. Evolution of $V_{P1\text{-}P2}$ and ΔV over time in the presence of a highly corroding area at different positions relative to the monitoring device. Input parameters: $i_{0,a}$ = 0.1 A m^{-2}, $i_{0,c}$ = 10^{-5} A m^{-2}, L_a = 7.5 cm, a = 5 cm, e = 40 mm, C_{dl} = 0.2 F m^{-2}, I_{C1} = 100 µA.

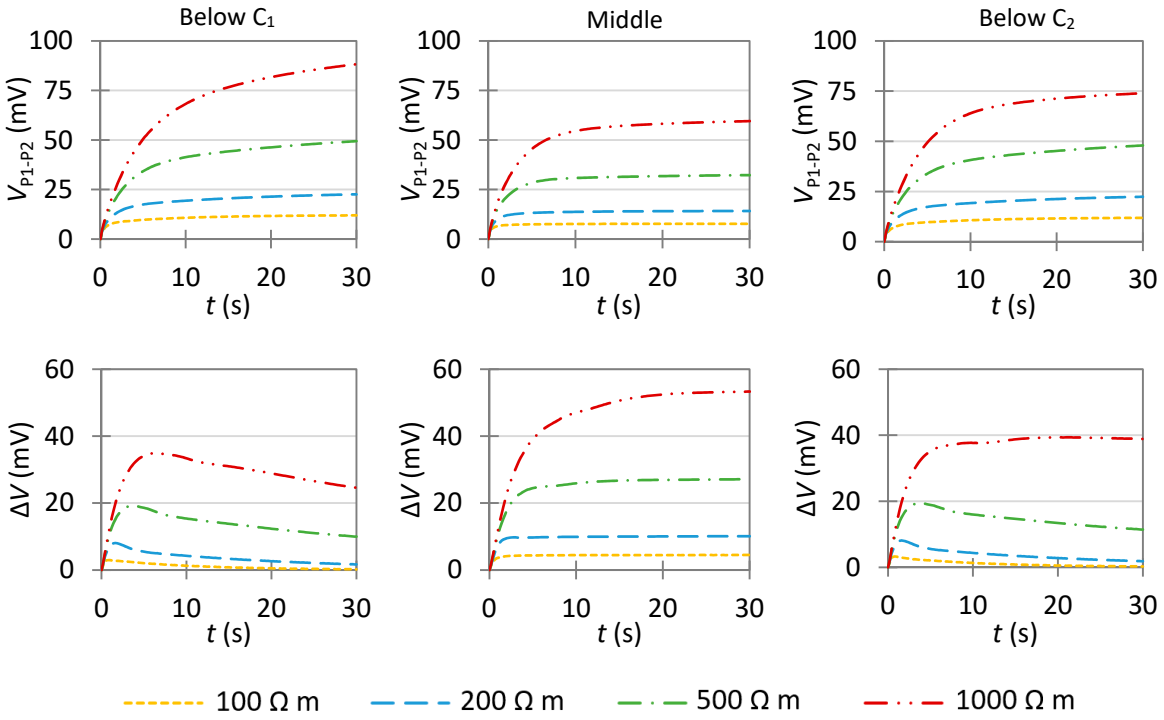

Figure S10C. Evolution of $V_{P1\text{-}P2}$ and ΔV over time in the presence of a highly corroding area at different positions relative to the monitoring device. Input parameters: $i_{0,a} = 0.1$ A m^{-2}, $i_{0,c} = 10^{-5}$ A m^{-2}, $L_a = 10$ cm, $a = 5$ cm, $e = 40$ mm, $C_{dl} = 0.2$ F m^{-2}, $I_{C1} = 100$ µA. Here, ΔV_{max} is greater when the anode is at the middle of the device.

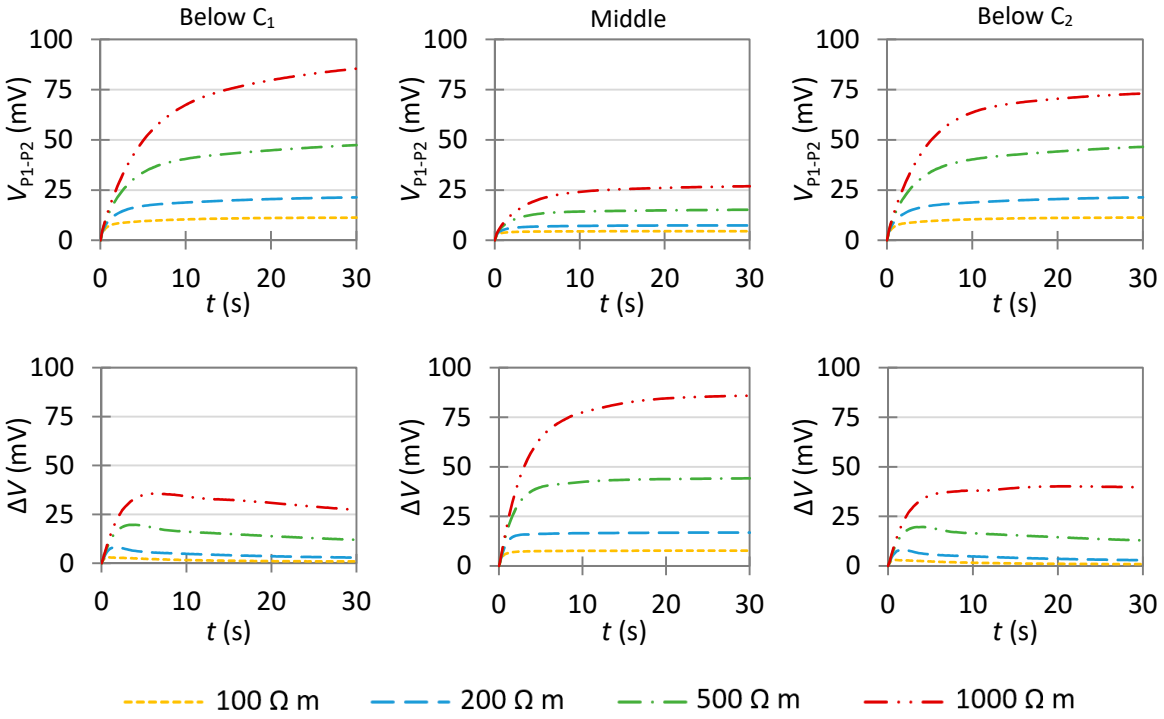

Figure S10D. Evolution of $V_{P1\text{-}P2}$ and ΔV over time in the presence of a highly corroding area at different positions relative to the monitoring device. Input parameters: $i_{0,a} = 0.1$ A m^{-2}, $i_{0,c} = 10^{-5}$ A m^{-2}, $L_a = 15$ cm, $a = 5$ cm, $e = 40$ mm, $C_{dl} = 0.2$ F m^{-2}, $I_{C1} = 100$ µA.

Figure S11

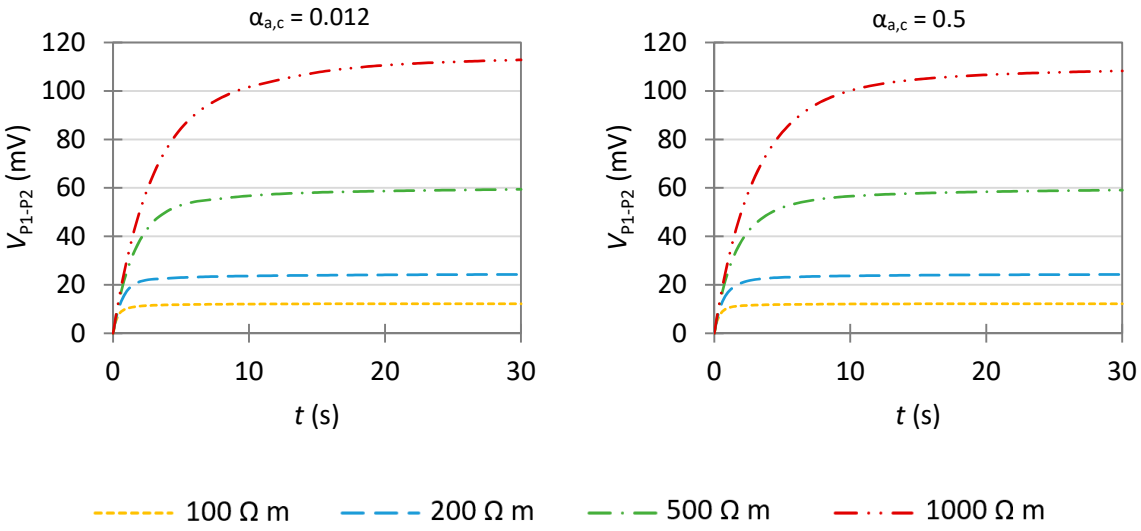

Figure S11A. Influence of the anodic charge transfer coefficient of the cathode $\alpha_{a,c}$ on the evolution of $V_{P1\text{-}P2}$ over time in uniform corrosion. Left: $\alpha_{a,c} = 0.012$; right: $\alpha_{a,c} = 0.5$. Input parameters: $i_0 = 10^{-5}$ A m^{-2}, $a = 5$ cm, $e = 40$ mm, $C_{dl} = 0.2$ F m^{-2}, $I_{C1} = 100$ µA.

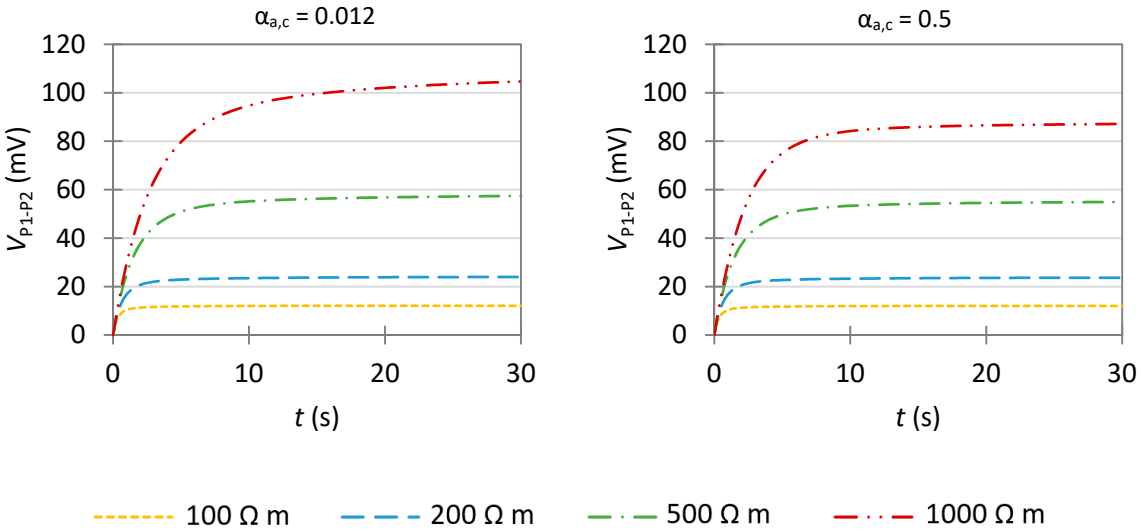

Figure S11B. Influence of the anodic charge transfer coefficient of the cathode $\alpha_{a,c}$ on the evolution of $V_{P1\text{-}P2}$ over time in uniform corrosion. Left: $\alpha_{a,c} = 0.012$; right: $\alpha_{a,c} = 0.5$. Input parameters: $i_0 = 10^{-4}$ A m^{-2}, $a = 5$ cm, $e = 40$ mm, $C_{dl} = 0.2$ F m^{-2}, $I_{C1} = 100$ µA.

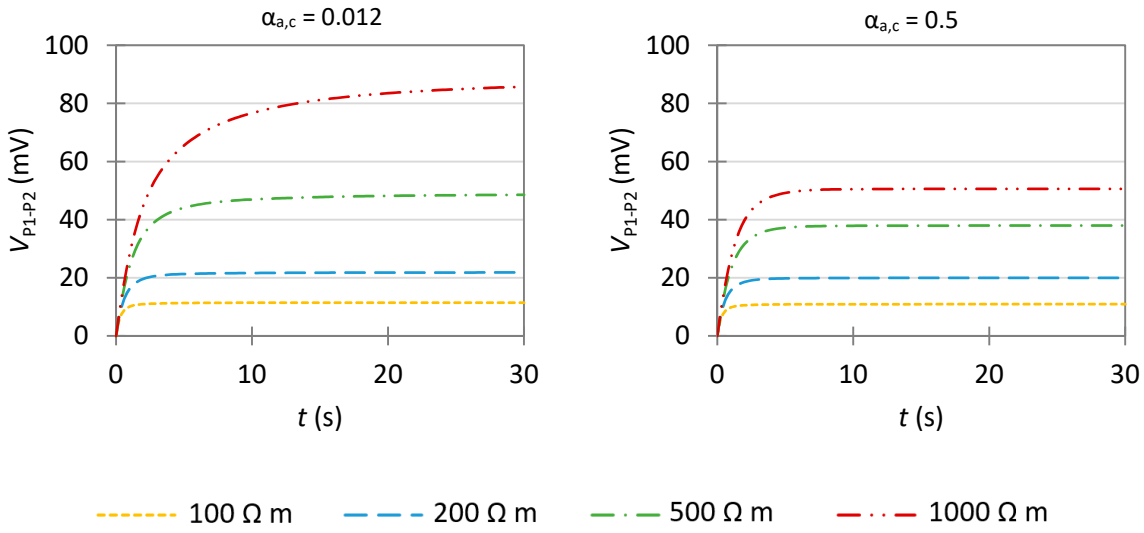

Figure S11C. Influence of the anodic charge transfer coefficient of the cathode $\alpha_{a,c}$ on the evolution of $V_{P1\text{-}P2}$ over time in uniform corrosion. Left: $\alpha_{a,c} = 0.012$; right: $\alpha_{a,c} = 0.5$. Input parameters: $i_0 = 10^{-3}$ A m^{-2}, $a = 5$ cm, $e = 40$ mm, $C_{dl} = 0.2$ F m^{-2}, $I_{C1} = 100$ µA.

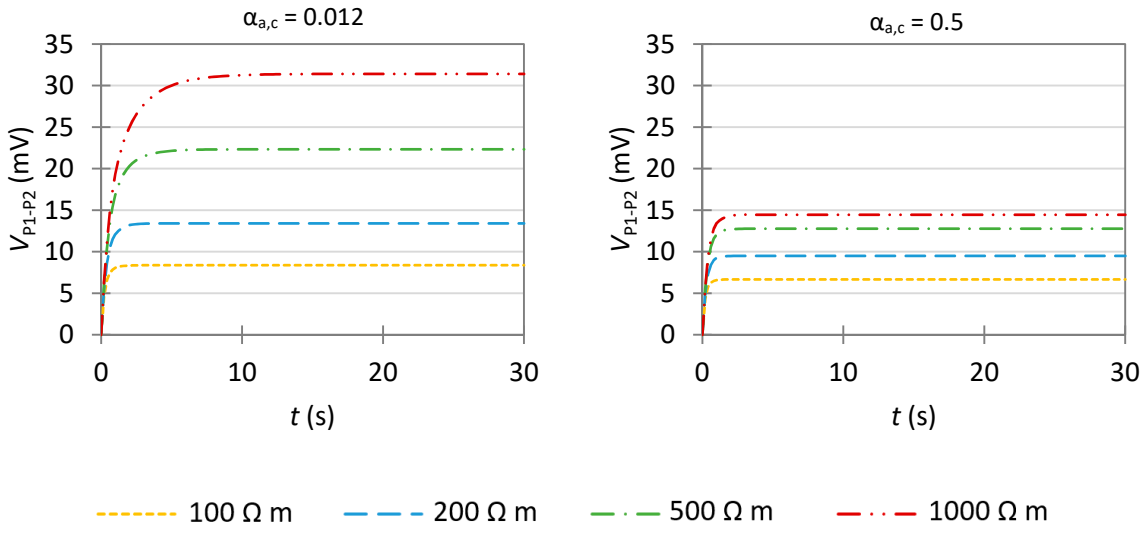

Figure S11D. Influence of the anodic charge transfer coefficient of the cathode $\alpha_{a,c}$ on the evolution of $V_{P1\text{-}P2}$ over time in uniform corrosion. Left: $\alpha_{a,c} = 0.012$; right: $\alpha_{a,c} = 0.5$. Input parameters: $i_0 = 10^{-2}$ A m^{-2}, $a = 5$ cm, $e = 40$ mm, $C_{dl} = 0.2$ F m^{-2}, $I_{C1} = 100$ µA.

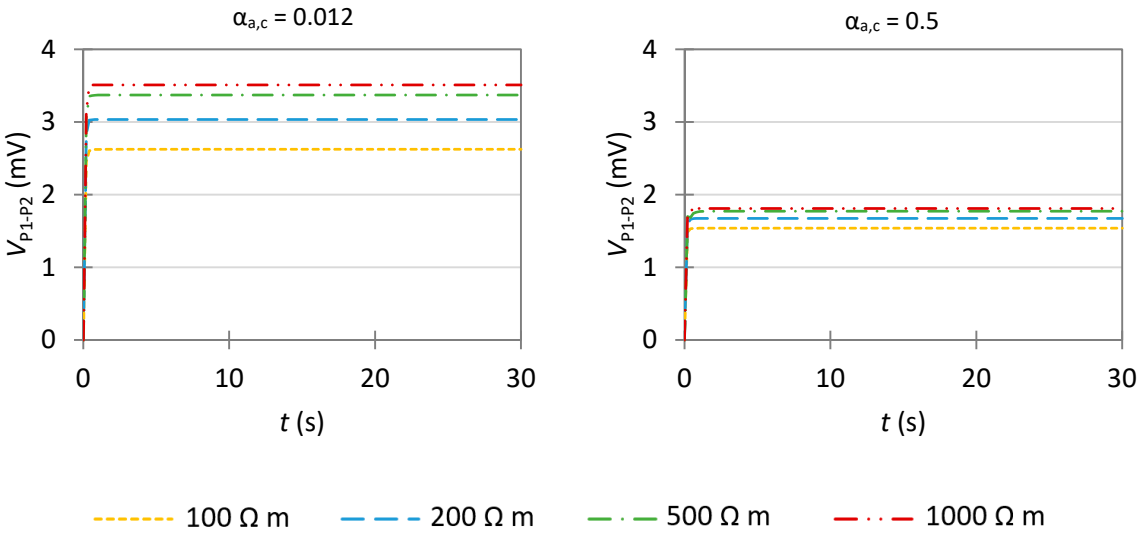

Figure S11E. Influence of the anodic charge transfer coefficient of the cathode $\alpha_{a,c}$ on the evolution of $V_{P1\text{-}P2}$ over time in uniform corrosion. Left: $\alpha_{a,c}$ = 0.012; right: $\alpha_{a,c}$ = 0.5. Input parameters: i_0 = 0.1 A m^{-2}, a = 5 cm, e = 40 mm, C_{dl} = 0.2 F m^{-2}, I_{C1} = 100 µA.